# Mirrors, lenses and Monge–Ampère equations

Quentin Mérigot and Boris Thibert

*Is it possible to shape a piece of glass so that it refracts and concentrates sunlight in order to produce a given image? The modelling of this kind of problem leads to nonlinear second-order partial differential equations, which belong to the family of Monge–Ampère equations. We will see how semi-discrete methods, that can be traced back to Minkowski's works, allow us to numerically solve such equations.*

## 1 Anidolic optics and Monge Ampère type equations

In anidolic optics, or non-imaging optics, one studies the design of devices that transfer light energy between a source and a target. The general problem is to design the shape of a mirror (or a lens) that reflects (or refracts) the light emitted from a given source towards a target whose geometry and intensity distributions are prescribed (see Figures 1 and 2). Applications of anidolic optics include the design of solar ovens, public lighting, car headlights, and more generally the optimization of the use of light energy and the reduction of light pollution.

### Near-field and far-field light sources

There exists many different problems in anidolic optics, depending for instance on the geometry of the light source, the type of optical component, and the target to be illuminated. These problems are distinguished in particular by the spatial position of the target illumination. A problem is called *near-field* when the target is located within a finite distance, i.e., when one wishes to illuminate an area of space such as a screen. In Figures 1 and 2, the target illumination is on a wall, making the problem near-field. Most of the illustrations in this article correspond near-field targets. However, we will first consider the *far-field* case, which is mathematically simpler, and
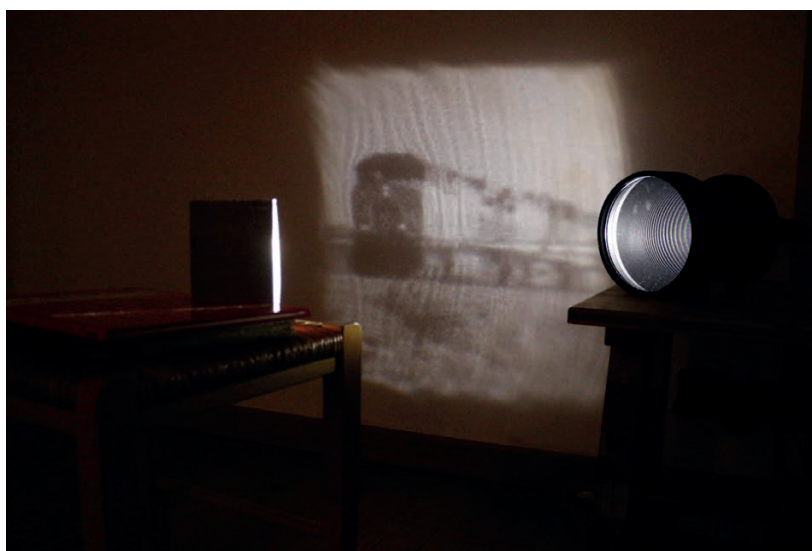


*Figure 1*. Mirror transforming a parallel, uniform light source into the shape of a train
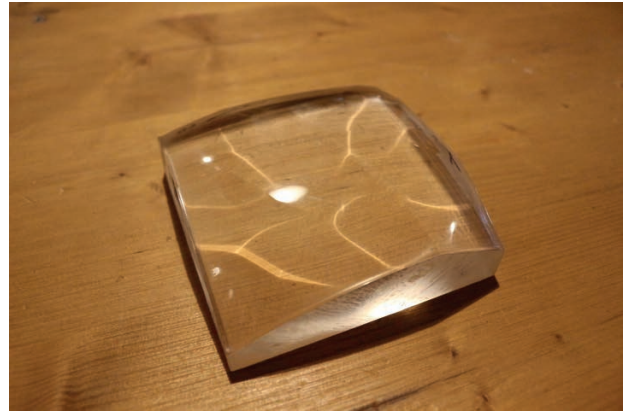
*Figure 2.* Lens transforming a parallel light source into a hikari

in which the target lies "at infinity", in the space of directions. In practice, this means that when light is reflected or refracted from a point of the optical component, we can forget the spatial position of the reflected or refracted ray, keeping only its direction, which can then be encoded by a unit vector. Note that if the near-field target illumination is far away from the optical component, each point of the target almost corresponds to a direction, so that the far-field problem is a good approximation of the near-field one in this situation. We will see in Section 4.2 that one can solve a problem involving a near-field target by iteratively solving problems with far-field targets.

We will first present two *far-field mirror problems* in their continuous form, as illustrated in Figure 3. Then, we will explain how these continuous problems can be approached by discrete problems, following the so-called *supporting quadric* method introduced by Luis Caffarelli and Vladimir Oliker. This method can be traced back to work of Hermann Minkowski and Aleksandr Aleksandrov in convex geometry.
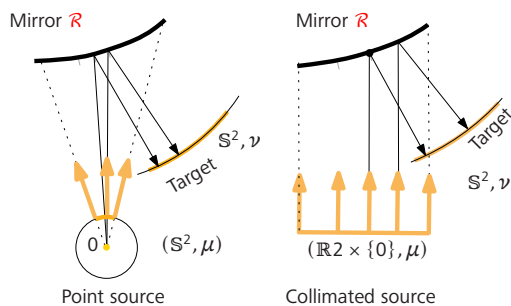


*Figure 3.* Mirror transforming light from a point source (left) or collimated light (right)

### 1.1 Mirror for a point light source

In this first problem, light is emitted from a point $O$, which we assume to be located at the origin of the space $\mathbb{R}^3$. The intensity of the light source is modeled by a probability density $\mu$ on the sphere of directions $\mathbb{S}^2$. Let $X \subset \mathbb{S}^2$ denote the support of the measure $\mu$. For example, if the light is emitted in a solid cone, then $X$ is a disc on the sphere. The quantity of light emanating from a measurable set of directions $A \subset X$ is given by $\mu(A)$. For the far-field problem, the target is described by a probability measure $\nu$ on the sphere of directions $\mathbb{S}^2$, which then represents the directions "at infinity", i.e., after reflection. Let $Y \subset \mathbb{S}^2$ denote the support of the measure $\nu$.

The inverse problem considered here consists in constructing the surface $\mathcal{R}$ of a mirror which will transport the intensity $\mu$ of the light source to the desired light distribution $\nu$ at infinity using Snell's law of reflection. For example, if the target measure is a Dirac mass $\delta_y$, meaning that we want to reflect all the light in a single direction $y$, then the shape of the mirror is given by a paraboloid of revolution.

Let $\langle \cdot | \cdot \rangle$ denote the Euclidean scalar product on $\mathbb{R}^3$. An incident ray $x \in \mathbb{S}^2$ is reflected by a surface $\mathcal{R}$ in the direction $R(x) = x - \langle x | n(x) \rangle n(x)$, where $n(x)$ is the unit vector normal to the surface $\mathcal{R}$ at the point touched by the direction $x$ and oriented so that $\langle x | n(x) \rangle \leq 0$. The surface $\mathcal{R}$ solves the inverse mirror problem if $R$ transports the source measure $\mu$ to the target measure $\nu$, in the sense that for any measurable subset $B$ of the sphere one has

$$\forall B \subseteq \mathbb{S}^2, \quad \nu(B) = \mu\big(R^{-1}(B)\big).$$

Note that the preservation of overall light quantity was already ensured by having chosen probability measures, i.e., $\mu(\mathbb{S}^2) = \nu(\mathbb{S}^2) = 1$. Now assume that $\mu$ and $\nu$ are absolutely continuous measures with respect to the area measure on the sphere. Let $\mu(x) = \rho(x)\mathrm{d}x$ and $\nu(x) = \sigma(x)\mathrm{d}x$, where $\rho$ and $\sigma$ are the densi-

ties of $\mu$ and $\nu$ respectively. The previous equation then reads

$$\forall B \subseteq \mathbb{S}^2, \quad \int_B \sigma(x)\,dx = \int_{R^{-1}(B)} \rho(x)\,dx. \tag{1}$$

Suppose furthermore that the densities $\rho$ et $\sigma$ are continuous and that $R$ is a diffeomorphism from $X$ to $Y$. By the change of variable $y = R(x)$, the last equation is then equivalent to $\sigma(R(x))\det(DR(x)) = \rho(x)$ for any $x \in X$.

Since the mirror reflects rays emitted from the origin, we will assume that the surface $\mathcal{R}$ is radially parametrized by $x \in \mathbb{S}^2 \mapsto u(x)x$, where $u : \mathbb{S}^2 \to \mathbb{R}^+$ is a positive function that must be determined. The unit normal to the surface $\mathcal{R}$ at the point $xu(x)$ and the direction of the reflected ray can both be expressed as a function of $x$ and of the gradient $\nabla u(x) \in T_x\mathbb{S}^2$:

$$R_u(x) = x - \langle x \mid n_u(x)\rangle n_u(x) \quad \text{and} \quad n_u(x) = \frac{\nabla u(x) - u(x)x}{\sqrt{\|\nabla u(x)\|^2 + u(x)^2}}.$$

This allows us to formulate the problem as a system of partial differential equations, i.e., the problem of finding a positive function $u : \mathbb{S}^2 \to \mathbb{R}^+$ of class $\mathcal{C}^2$ which satisfies

$$\begin{cases} \sigma(R_u(x))\det(DR_u(x)) = \rho(x), \\ R_u \text{ be a diffeomorphism from } X \text{ to } Y. \end{cases} \tag{Mir-Ponc-C}$$

The first line of equation (Mir-Ponc-C) involves the determinant of a quantity which depends on the second derivatives of $u$. This equation belongs to the family of Monge–Ampère equations. Note that the requirement that $R_u$ is a diffeomorphism is non-standard and difficult to handle. In practice, it is replaced by a condition on $u$ which is akin to convexity, and by the so-called second boundary condition $R_u(X) = Y$. These two conditions ensure the ellipticity of the problem. Caffarelli and Oliker proved in 1994 [1] the existence of weak solutions to this equation, i.e., the existence of a locally Lipschitz function $u$ such that the application $R$ defined by the last two lines of (Mir-Ponc-C) satisfies (1). The existence of regular solutions to the problem (Mir-Ponc-C) is due to Wang and Guan [2, 6].

### 1.2  Mirror for a collimated light source

We now present a second inverse problem arising in anidolic optics. This time the light source is collimated, which means that all the rays of light emitted by the source are parallel. We furthermore assume that they are positively collinear to the vertical vector $e_z = (0, 0, 1)$ and emitted from a domain of the horizontal plane $X \subset \mathbb{R}^2 \times \{0\}$. For convenience, we will identify $\mathbb{R}^2$ and $\mathbb{R}^2 \times \{0\}$. We assume that the surface of the optical component is smooth and parametrized by a height function $u : X \to \mathbb{R}$. The intensity of the light source is modeled by a probability measure $\mu$ on $X$. As in the previous case, the intensity of the target illumination is modeled by a probability measure $\nu$ on the sphere of directions

at infinity. At each point $(x, u(x))$ of the optical component, the gradient $\nabla u(x)$ encodes the direction of the normal to the surface and we denote by $F(\nabla u(x)) \in \mathbb{S}^2$ the direction of the ray reflected by Snell's law. The reflector defined by $u$ solves the inverse mirror problem between $\mu$ and $\nu$ if for any measurable set $B \subset \mathbb{S}^2$ one has

$$\nu(B) = \mu\big((F \circ \nabla u)^{-1}(B)\big).$$

Let us introduce the measure $\tilde{\nu}$ defined by $\tilde{\nu}(B) = \nu(F(B))$, which is supported on $\mathbb{R}^2$. We assume that $\mu$ and $\tilde{\nu}$ are absolutely continuous with respect to the Lebesgue measure, with continuous densities $\rho$ and $\sigma$, and that $x \mapsto \nabla u(x)$ is a diffeomorphism on its image. Then, with the change of variable $y = \nabla u(x)$, the inverse mirror problem for a collimated source can also be phrased as a partial differential equation:

$$\begin{cases} \sigma(\nabla u(x))\det(D^2 u(x)) = \rho(x), \\ F \circ \nabla u \text{ is a diffeomorphism from } X \text{ to } Y. \end{cases} \tag{Mir-Coll-C}$$

We finally note that if $u$ is smooth and strongly convex (or strongly concave), the application $\nabla u$ is a diffeomorphism on its image.

### 1.3  Lenses

The construction of lenses that transform a light source into a target illumination prescribed at infinity are similar and are also described by Monge–Ampère type equations. As with mirrors, when the light is emitted from a point, the equation to be solved is on the sphere and when the light source is collimated, it is on the plane. In these problems, the light source passes through the surface of one side of the lens, either flat or spherical, and the aim is to construct the surface of the other side of the lens such that it refracts the light onto a prescribed target illumination at infinity. We do not detail the modelling of these problems here, but we will show results with lenses at the end.

## 2  Geometric discretization of Monge–Ampère equations

The two inverse problems in anidolic optics described in the previous section each involve two sets $X$ and $Y$, on which we have two probability measures $\mu$ and $\nu$ respectively, representing the light source and the desired target illumination. We saw that when these measures are absolutely continuous, the problems of construction of optical components correspond to partial differential equations of Monge–Ampère type.

The most direct method to solve a partial differential equation numerically is to approximate the domain $X$ with a discrete grid and to replace the partial derivatives with differences of the values of the function at the points of the grid divided by the grid step. In the

case of Monge–Ampère equations, the application of these methods is made difficult by the non-linearity of the Monge–Ampère operator and by the diffeomorphism condition. We refer to the work of Adam Oberman, Brittany Froese, Jean-David Benamou and Jean-Marie Mirebeau for this line of research.

In recent years, alternative methods, called *semi-discrete* methods, have been used to discretize and numerically solve Monge–Ampère type equations arising from optimal transport. In order to apply this method, one assumes that one of the two measures $\mu$ or $\nu$ is absolutely continuous, while the other is finitely supported. Here we assume that $\mu$ has a density $\mu(x) = \rho(x)\,dx$ on the space $X$ and that $\nu$ is a discrete measure on the space $Y = \{y_1, \ldots, y_N\}$, i.e., $\nu = \sum_{1 \le i \le N} \delta_{y_i} \nu_i$ where $\delta_{y_i}$ is the Dirac mass in $y_i$.

In this section, we describe the semi-discrete variant of the two far-field mirror problems seen in the previous section, leaving aside the problem of convergence of the solutions to the discrete problems towards those to the continuous problems. These constructions give rise to equations which can naturally be seen as *discrete Monge–Ampère equations*. We also propose an economic interpretation by addressing the *bakeries problem*.

### 2.1 Mirror for a point light source

Let us go back to the problem of constructing mirrors that transform the light emitted by a point light source (see Section 1.1). As in the previous section, the light source is modeled by a continuous probability density $\rho$ on the sphere of directions $\mathbb{S}^2$, whose support $X_\rho := \{x \in \mathbb{S}^2, \rho(x) > 0\}$ corresponds to the set of directions in which light is emitted. This time we assume that the desired target illumination is described by a probability measure $\nu = \sum_{1 \le i \le N} \delta_{y_i} \nu_i$ supported on a set $Y = \{y_1, \ldots, y_N\} \subset \mathbb{S}^2$ of distinct directions. The problem is still to find the mirror surface $\mathcal{R}$ that will reflect the measure $\mu$ onto the measure $\nu$ under Snell's law, but this time the target measure $\nu$ is discrete.

### Mirror composed of paraboloid pieces

We use the method of *supporting paraboloids* proposed by Caffarelli and Oliker in 1994 [1], which was originally developed to show the existence of weak solutions in the case where both measures are absolutely continuous. Caffarelli and Oliker's idea is based on a well-known property of paraboloids of revolution: a paraboloid of revolution with focal point $O$ and direction $y$ reflects any ray coming from point $O$ to the direction $y$. It is thus natural to seek to construct a mirror whose surface is composed of pieces of paraboloids, each paraboloid illuminating a direction $y_i$.

More precisely, we take $\psi = (\psi_1, \ldots, \psi_N) \in \mathbb{R}^N$ and denote by $P(y_i, \psi_i)$ the solid (i.e. filled) paraboloid of direction $y_i$, with focal point at the origin $O$ and focal distance $\psi_i$. This means that $\frac{1}{2}\psi_i$ is the distance between $O$ and the paraboloid's closest point to $O$.

We define by $\mathcal{R}_\psi$ the surface bordering the intersection of the solid paraboloids $P(y_i, \psi_i)$:

$$\mathcal{R}_\psi = \partial\left(\bigcap_{1 \le i \le N} P(y_i, \psi_i)\right).$$

For each $i \in \{1, \ldots, N\}$ we denote by $V_i(\psi)$ the set of rays $x \in \mathbb{S}^2$ emitted by the light source and reflected by Snell's law in the direction $y_i$. This set is called the *i*-th *visibility cell of the mirror* $\mathcal{R}_\psi$. By construction, it corresponds to the radial projection of $\mathcal{R}_\psi \cap \partial P(y_i, \psi_i)$ onto the sphere (see Figure 4).

A simple calculation shows that the intersection of two confocal paraboloids $\partial P(y_i, \psi_i)$ and $\partial P(y_j, \psi_j)$ is included in a plane curve. Projecting radially onto the unit sphere, this implies that the intersection of two visibility cells $V_i(\psi) \cap V_j(\psi)$ is included in a curve on the sphere. We deduce that the set of visibility cells forms a partition of the sphere $\mathbb{S}^2$, up to a set of measure zero.

The paraboloid of revolution $\partial P(y_k, \psi_k)$ can be parametrized radially by the function $x \in \mathbb{S}^2 \mapsto x\rho_k(x)$, where $\rho_k(x) = \psi_k/(1 - \langle x|y_i\rangle) \in \mathbb{R}$. We deduce that $x$ belongs to the visibility cell $V_i(\psi)$ if and only if the distance $\rho_i(x)$ is smaller than the distances $\rho_j(x)$ for $j \in \{1, \ldots, N\}$. Composing with the logarithm to linearize the expression in $\psi$, we obtain an explicit expression for the visibility cells

$$V_i(\psi) = \left\{x \in \mathbb{S}^2 \mid \forall j, \ c(x, y_i) + \ln(\psi_i) \le c(x, y_j) + \ln(\psi_j)\right\},$$

where $c(x, y) = -\ln(1 - \langle x|y\rangle)$.

By construction, each ray emitted by the point source and belonging to the cell $V_i(\psi)$ hits the mirror $\mathcal{R}_\psi$ at a point which belongs to the paraboloid $\partial P(y_i, \psi_i)$ and which is reflected in the direction $y_i$. The quantity of light received in the direction $y_i$ is therefore exactly the quantity of light emanating from the visibility cell $V_i(\psi)$, i.e., $\mu(V_i(\psi))$. The desired quantity of light in the direction $y_i$ is $\nu_i$. The equation to be solved is therefore $\mu(V_i(\psi)) = \nu_i$ for any $i \in \{1, \ldots, N\}$. Moreover, note that a paraboloid of revolution is only determined by its focal point, its direction and its focal distance. The free parameter remaining for each paraboloid $\partial P(y_i, \psi_i)$ is the focal distance $\psi_i$.
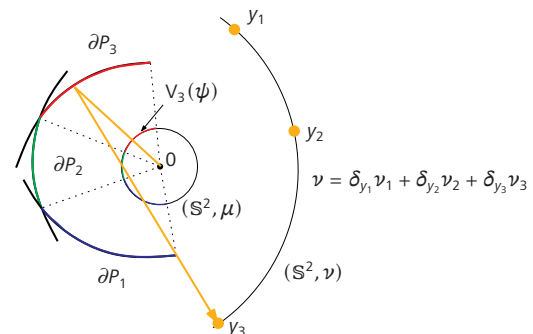


*Figure 4.* Mirror composed of three pieces of paraboloides reflecting in three directions

*Formulation of the problem*

The semi-discrete far-field mirror problem for a point source can be formulated as the problem of finding focal distances $\psi = (\psi_1, \ldots, \psi_N) \in \mathbb{R}^N$ that satisfy

$$\forall i, \quad \mu(V_i(\psi)) = \nu_i \qquad \text{(Mir-Ponc-SD)}$$

where $c(x,y) = -\ln(1 - \langle x | y \rangle)$ and where

$$V_i(\psi) = \left\{ x \mid \forall j, \; c(x, y_i) + \ln(\psi_i) \leq c(x, y_j) + \ln(\psi_j) \right\}.$$

We will see in Section 3 how to solve such systems of equations. Note that if $\psi \in \mathbb{R}^N$ is a vector of focal distances solving the mirror problem for a point-like source, then the surface of the mirror is parametrized by

$$\mathcal{R}_\psi : x \in \mathbb{S}^2 \mapsto \min_i \frac{\psi_i}{1 - \langle x | y_i \rangle} \, x.$$

In the numerical experiments, we assume that the target illumination $\nu$ is included in the half-sphere $\mathbb{S}^2_- := \{x \in \mathbb{S}^2, \; \langle x | e_z \rangle \leq 0\}$, that the support $X_\rho$ of $\rho$ is included in the half-sphere $\mathbb{S}^2_+ := \{x \in \mathbb{S}^2, \; \langle x | e_z \rangle \geq 0\}$, and that the mirror is parametrized above the domain $X_\rho$.

**Remark 2.1.** The mirror surface is by construction the boundary of a convex set, i.e., the intersection of the solid paraboloids $P(y_1, \psi_1), \ldots, P(y_N, \psi_N)$. It is also possible to construct a mirror contained in the boundary of the union of solid paraboloids rather than an intersection. This produces mirrors that are somewhat less interesting in practice, as they are neither convex nor concave.

## 2.2 Mirror for a collimated light source

Let us now consider the mirror problem for a collimated light source, already seen in Section 1.2. As before, the probability measure modelling the light source has a density $\rho$ with respect to the Lebesgue measure on the plane. However the probability measure modelling the target illumination intensity is discrete $\nu = \sum_{1 \leq i \leq N} \delta_{y_i} \nu_i$, supported on a finite set $Y = \{y_1, \ldots, y_N\} \subset \mathbb{S}^2$ of distinct directions. The problem is, again, to find the surface $\mathcal{R}$ of a mirror which reflects the measure $\mu$ to the measure $\nu$.

*Mirror with planar faces*

We choose to construct the mirror surface $\mathcal{R}$ as the graph of affine height functions of the form $x \in \mathbb{R}^2 \mapsto \max_i \langle x | p_i \rangle - \psi_i$ (see Figure 5). The vector $p_i$ is chosen so that the plane $P_i = \{(x, \langle x | p_i \rangle) \mid x \in \mathbb{R}^2\}$ reflects vertical rays, i.e., with direction $e_z$, into the direction $y_i \in \mathbb{S}^2$. We need to determine the heights $\psi_i$ of those planes. Given a family of heights $\psi \in \mathbb{R}^N$, we define the $i$-th visibility cell as

$$V_i(\psi) = \{x \in \mathbb{R}^2 \times \{0\} \mid \forall j, \; -\langle x | p_i \rangle + \psi_i \leq -\langle x | p_j \rangle + \psi_j\}.$$
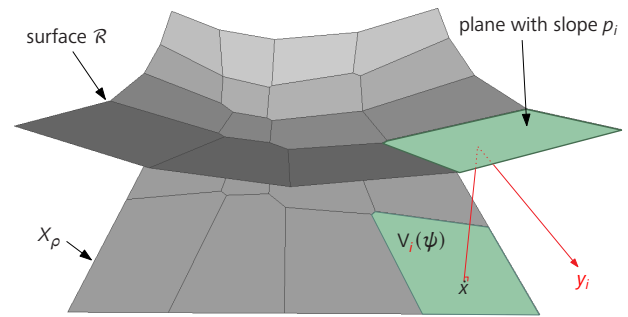


*Figure 5.* Convex mirror for a collimated light source

By construction, for each $i \in \{1, \ldots, N\}$, any vertical ray emitted from a point $x \in V_i(\psi)$ hits the mirror $\mathcal{R}$ at a height $\langle x | p_i \rangle - \psi_i$ and is reflected in the direction $y_i$. Thus, the amount of light reflected in the direction $y_i$ is equal to $\mu(V_i(\psi))$.

*Formulation of the problem*

Solving the semi-discrete far-field mirror problem for a collimated light source amounts to finding the heights $\psi \in \mathbb{R}^N$ that satisfies

$$\forall i, \quad \mu(V_i(\psi)) = \nu_i \qquad \text{(Mir-Colli-SD)}$$

where $c(x,y) = -\langle x | y \rangle$ and

$$V_i(\psi) = \left\{ x \mid \forall j, \; c(x, y_i) + \psi_i \leq c(x, y_j) + \psi_j \right\}.$$

A solution of the equation (Mir-Colli-SD) induces a parametrization of the convex mirror $\mathcal{R}$ that reflects $\mu$ onto $\nu$:

$$\mathcal{R}_\psi : x \in \mathbb{R}^2 \mapsto \left(x, \max_i \langle x | p_i \rangle - \psi_i\right) \in \mathbb{R}^3.$$

In practice, we only consider the part of the mirror located above the domain $X_\rho := \{x \in \mathbb{R}^2 \times \{0\}, \; \rho(x) \neq 0\}$.

**Remark 2.2.** The function $\mathcal{R}_\psi$ being the maximum of affine functions, it is convex. The optical component which is parametrized by the graph of this application is also convex. Note that one could have the same construction by replacing the max in the formula by a min. This would result in a concave function $\mathcal{R}_\psi$ and a concave mirror.

**Remark 2.3.** Problem (Mir-Colli-SD) is very similar (but not equivalent) to Minkowski's problem in convex geometry which is also an inverse problem. Given a set of unit vectors $y_i$ and real numbers $\nu_i > 0$, this problem consists in building a convex polyhedron whose $i$-th facet has normal $y_i$ and area $\nu_i$ – which is possible only under some assumptions on the directions and areas. We also note that Oliker, who was the first to introduce semi-discrete methods for the numerical resolution of Monge–Ampère equations, was a doctoral student of the famous geometer Aleksandrov who is known (among other) for introducing and studying the "continuous" formulation of Minkowski's problem.

## 2.3 The bakeries problem

We now present an economic analogy which leads to an equation having the same structure as in the two optical problems presented above. We assume that $X$ represents a city whose population density is described by a probability density $\rho$, that the finite set $Y = \{y_1, \ldots, y_N\}$ represents the locations of the city's bakeries and that $\nu_i$ represents the quantity of bread available in bakery $y_i$. Customers living at a location $x$ in $X$ naturally will look for the bakery minimizing the cost of walking from $x$ to $y_i$, denoted $c(x, y_i)$. This leads to a decomposition of the city space into *Voronoi cells*,

$$\text{Vor}_i := \{x \in \Omega_X \mid \forall j, \ c(x, y_i) \le c(x, y_j)\}.$$

The number of customers going to a bakery $y_i$ is equal to the integral of the density $\rho$ over $\text{Vor}_i$. Suppose that a bakery $y_i$ receives too many customers in comparison to its bread's production capacity $\nu_i$ – this could be the case in Figure 6 for the downtown bakery $y_1$ where the population density is high. This means we have $\mu(\text{Vor}_1) > \nu_1$, where we denote $\mu(x) = \rho(x)\text{d}x$. The baker $y_1$ will then seek to increase the price of his bread. This will reduce the number of potential customers, but will increase the baker's profit as long as he manages to sell all his stock. We write $\nu_i \ge 0$ for the proportion of the population that the bakery $y_i$ is able to serve, and $\psi_i$ the price of the bread in the bakery $y_i$. If we assume that the customers living at point $x$ make a compromise between walking cost and price of bread by minimizing the sum $(c(x, y_i) + \psi_i)$, the city is then decomposed into *Laguerre cells*

$$\text{Lag}_i(\psi) = \{x \in X \mid \forall j, \ c(x, y_i) + \psi_i \le c(x, y_j) + \psi_j\}.$$

Note that we do not necessarily have $y_i \in \text{Lag}_i(\psi)$, and that it is even possible to have $\text{Lag}_i(\psi) = \varnothing$: indeed, if the bread is very expensive in a certain bakery, even people living next door may prefer going to a more distant one.

*Problem formulation*

The bakeries problem therefore boils down to finding a price vector $\psi \in \mathbb{R}^N$ such that each bakery sells all its stock of bread $\nu_i$. This is described by the system of equations

$$\mu(\text{Lag}_i(\psi)) = \nu_i \quad \forall i \in \{1, \ldots, N\},$$

This equation has exactly the same structure as (Mir-Ponc-SD) and (Mir-Colli-SD). We will see in the next section how to solve this class of equations.

## 3 Numerical resolution

The discrete problems mentioned in the previous section all show the same structure; our focus will now be on their numerical resolution. We start by introducing the semi-discrete Monge–Ampère equation, and show that its solution is equivalent to finding the maximum of a concave function. Subsequently, we present a Newton method that allows us to solve these equations efficiently.

## 3.1 Semi-discrete Monge–Ampère equation

Let $X$ be a compact subset of the space $\mathbb{R}^2$ or of the sphere $\mathbb{S}^2$, let $Y = \{y_1, \ldots, y_N\}$, and let $c \in \mathcal{C}^1(X \times Y)$ be a cost function. The *Laguerre cell* (which corresponds to a visibility cell in optics) associated with a family of real numbers $\psi = (\psi_1, \ldots, \psi_N) \in \mathbb{R}^N$ is given by

$$\text{Lag}_i(\psi) = \{x \in X \mid \forall j, \ c(x, y_i) + \psi_i \le c(x, y_j) + \psi_j\}.$$

Suppose that the cost function satisfies the *Twist condition*

$$\forall x \in X, \quad y \mapsto \nabla_x c(x, y) \text{ is injective}, \qquad \text{(Twist)}$$

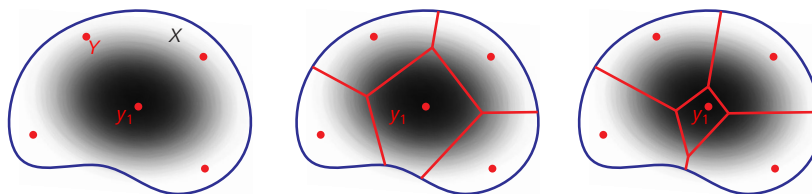which ensures that the Laguerre cells form a partition of the domain $X$ up to a negligible set.



Figure 6. Bakeries: The city $X$ with its boundary drawn in blue is endowed with a probability density pictured in grayscale representing the population density. The set $Y$ (in red) represents the location of bakeries. Here, $X, Y \subseteq \mathbb{R}^2$ and $c(x, y) = |x - y|^2$. We see the Voronoi tessellation of the city (in the middle, uniform price) as well as its Laguerre tessellation (on the right, only the bread price $\psi_1$ has increased).

*Semi-discrete Monge–Ampère equation*

Let $\mu$ be a probability measure on $X$ with density $\rho$ with respect to the area measure, and let $\nu = \sum_i \nu_i \delta_{y_i}$ be a probability measure on $Y$. In the following equation, the discrete probability measure $\nu$ is conflated with the vector $\nu = (\nu_i)_{1 \le i \le N}$. We are seeking $\psi \in \mathbb{R}^N$ satisfying

$$G(\psi) = \nu, \qquad (\text{MA})$$

where the function $G : \mathbb{R}^N \to \mathbb{R}^N$ is defined by

$$G(\psi) = (G_1(\psi), \dots, G_N(\psi)) \quad \text{and} \quad G_i(\psi) = \mu(\text{Lag}_i(\psi)).$$

**Remark 3.1.** The visibility cells used in optics in (Mir-Ponc-SD) and (Mir-Colli-SD) are Laguerre cells, with

$$c(x, y) = -\log(1 - \langle x|y \rangle) \quad \text{and} \quad c(x, y) = -\langle x|y \rangle$$

respectively. Equation (MA) is a reformulation of equations (Mir-Ponc-SD) and (Mir-Colli-SD). Note that the Laguerre cells are invariant under addition of a constant to $\psi$, and that the solution of (MA) is therefore defined up to an additive constant. Optical problems have a similar invariance: for example, if a surface $\mathcal{R}$ is a solution of the mirror problem for a point source, then so is $\lambda \mathcal{R}$ for all $\lambda > 0$.

## 3.2 Variational formulation

The following theorem shows that the function $G$ in the semi-discrete Monge–Ampère equation is the gradient of a concave function.

**Theorem 3.1.** *We assume that the cost function $c$ satisfies* (Twist). *Then the function $\mathcal{K} : \mathbb{R}^N \to \mathbb{R}$ defined by*

$$\mathcal{K}(\psi) = \sum_{1 \le i \le N} \int_{\text{Lag}_i(\psi)} (c(x, y) + \psi_i) \rho(x) dx - \sum_{1 \le i \le N} \psi_i \nu_i$$

*is concave, of class $\mathcal{C}^1$ and with gradient*

$$\nabla \mathcal{K}(\psi) = G(\psi) - \nu = (\mu(\text{Lag}_i(\psi)) - \nu_i)_{1 \le i \le N}.$$

As we will see in the next paragraph, the function $\mathcal{K}$ is related to the Kantorovitch duality in optimal transport theory, and we will therefore call it the *Kantorovitch functional*. Moreover, since a concave function of class $\mathcal{C}^1$ reaches its maximum exactly at its critical points, we obtain the following corollary:

**Corollary 3.2.** *Under the assumptions of Theorem* 3.1, *a vector $\psi \in \mathbb{R}^N$ is a solution to equation* (MA) *if and only if $\psi$ is a maximizer of $\mathcal{K}$.*

Since the function $\mathcal{K}$ is invariant under addition of a constant, one can choose to work on the set $\mathcal{M}_0$ of vectors whose coordinates sum to zero. It can be shown that the function $\mathcal{K}$ is proper on $\mathcal{M}_0$, i.e., $\lim_{\|\psi\| \to +\infty, \psi \in \mathcal{M}_0} \mathcal{K}(\psi) = -\infty$, which ensures that it reaches its maximum: the problem (MA) thus admits a solution.

## 3.3 Relation to optimal transport

The variational formulation of the Monge–Ampère equation, i.e., the search for a maximizer of the Kantorovitch functional, corresponds in fact to the dual of the Monge–Kantorovitch problem in optimal transport theory. We discuss this link in detail below in the semi-discrete case. The reader interested in the proofs may refer for instance to the book chapter [4].

*Monge's problem*

The image of a probability measure $\mu$ on $X$ under a measurable application $T : X \to Y$ is the measure $T_\# \mu$ on $Y$ defined by $T_\# \mu(B) = \mu(T^{-1}(B))$. If $T_\# \mu = \nu$, we say that $T$ *transports* $\mu$ to $\nu$. Since the set $Y$ is finite, we have $T_\# \mu = \sum_{1 \le i \le N} \mu(T^{-1}(y_i)) \delta_{y_i}$. Monge's optimal transport problem consists in finding a transport map $T$ that transports $\mu$ to $\nu$ and that minimizes the total cost $\int_X c(x, T(x)) d\mu(x)$. If the cost function $c$ satisfies the Twist condition, Brenier and Gangbo–McCann, relying on Kantorovich duality, proved the existence of a minimizer for this problem when the source $\mu$ is absolutely continuous. For example, one can state the following:

**Theorem 3.3** (Kantorovitch duality). *Suppose that $c$ satisfies the condition* (Twist) *and that $\mu$ is absolutely continuous. Then*

$$\min_{\substack{T : X \to Y \\ T_\# \mu = \nu}} \int_X c(x, T(x)) d\mu(x) = \max_{\psi \in \mathbb{R}^N} \mathcal{K}(\psi).$$

*If moreover $\psi$ is a maximizer of $\mathcal{K}$, then the function $T_\psi : X \to Y$ defined $\mu$-a.e. by $T_\psi|_{\text{Lag}_y(\psi)} = y$ realizes the minimum in Monge's problem.*

**Remark 3.2.** Not all Monge–Ampère equations derive from an optimal transport problem and not all of them admit a variational formulations. These two strong properties come in fact from the very particular structure of Laguerre cells, which follows from the functions $\psi \mapsto c(x, y) + \psi(y)$ being affine.

We saw that the far-field optics problems presented in Section 2 possess this structure. On the other hand, if we consider the mirror construction problems for a target illumination in the near-field (i.e., we are illuminating points in $\mathbb{R}^3$ and not directions at infinity), we still have semi-discrete Monge–Ampère equations to solve, but the Laguerre cells are of the form

$$\text{Lag}_i(\psi) = \{x \in X \mid \forall j, \ G(x, y_i, \psi_i) \le G(x, y_j, \psi_j)\},$$

where the function $G$ is nonlinear in $\psi$. These equations do not derive from the optimal transport problem and in fact do not admit a variational formulation. They are called *prescribed Jacobian equations* by Trudinger, and are the subject of recent research both in analysis and in more applied fields (optics, economics).

### 3.4 Laguerre cells and derivatives

Before applying Newton's method to solve the equation $G(\psi) = \nu$, we need to show that the function $G$ is of class $\mathcal{C}^1$ (or equivalently that $\mathcal{K}$ is of class $\mathcal{C}^2$), calculate its partial derivatives and study the (strict) concavity of $\mathcal{K}$. To do this, we need a genericity assumption which is somewhat technical, but which is natural and not restrictive in practice. In the optical cases mentioned in this paper, this assumption is satisfied if the intersection of three distinct Laguerre cells is finite and if the intersection of two Laguerre cells with the boundary of $X$ is also finite. For more details, the reader may refer to the book chapter [4].

**Theorem 3.4** (Differential of $G$). *Suppose that the cost satisfies* (Twist), *that $Y$ is generic (see above), and $\rho$ is continuous. Then the application $G : \mathbb{R}^N \to \mathbb{R}^N$ is of class $\mathcal{C}^1$ and*

$$\forall j \neq i, \quad \frac{\partial G_i}{\partial \psi_j}(\psi) = \int_{\mathrm{Lag}_{ij}(\psi)} \frac{\rho(x)}{\left\| \nabla_x c(x, y_i) - \nabla_x c(x, y_j) \right\|} \, dx,$$

$$\forall i, \quad \frac{\partial G_i}{\partial \psi_i}(\psi) = -\sum_{j \neq i} \frac{\partial G_i}{\partial \psi_j}(\psi),$$

*where* $\mathrm{Lag}_{ij}(\psi) = \mathrm{Lag}_i(\psi) \cap \mathrm{Lag}_j(\psi)$.

The formula for the partial derivatives of $G$ has a geometric interpretation. In the following two figures, which are obtained for the cost $c(x, y) = \|x - y\|^2$ on $\mathbb{R}^2$, we explain why the formula for partial derivatives involves integrals over the interfaces between Laguerre cells and how the singularities of $DG$ may occur depending on the geometry of the points $y_i$.

Figure 7 illustrates that the partial derivative $\partial G_i / \partial \psi_j(\psi)$ is an integral over the interface $\mathrm{Lag}_{ij}(\psi)$: the value $G_i(\psi)$ is an integral over the Laguerre cell $\mathrm{Lag}_i(\psi)$ (in grey on the left); we increase the value $\psi_j$ by $\varepsilon > 0$ considering $\psi + \varepsilon e_j$; the rate of increase $(G_i(\psi) - G_i(\psi + \varepsilon e_j))/\varepsilon$ is proportional to an integral over the symmetric difference between two Laguerre cells (in grey in the middle); passing to the limit we obtain an integral over the green segment $\mathrm{Lag}_{ij}(\psi)$. The signs that occurs in the formula for the partial derivatives can also be interpreted with the bakeries metaphor: when the price of bread $\psi_i$ increases, the number of customers of the bakery $y_i$ decreases (i.e., the Laguerre cell $\mathrm{Lag}_i(\psi)$ shrinks) and the number of customers for the other bakeries increases, so that $\partial G_i / \partial \psi_i(\psi) \leq 0$ and $\partial G_i / \partial \psi_j(\psi) \geq 0$ for $j \neq i$.

In Figure 8, the genericity condition is not satisfied because $y_1$, $y_2$ and $y_3$ are aligned, and there exists $\psi \in \mathbb{R}^N$ for which $\mathrm{Lag}_1(\psi) \cap \mathrm{Lag}_2(\psi) \cap \mathrm{Lag}_3(\psi)$ is a line segment. The partial derivative $\partial G_2 / \partial \psi_3(\psi)$ is an integral on the (green) segment $\mathrm{Lag}_{23}(\psi)$. If we simultaneously decrease $\psi_1$ and $\psi_2$ by the same amount, we can see that the segment $\mathrm{Lag}_{23}(\psi)$ varies continuously and then suddenly becomes empty when the cell $\mathrm{Lag}_2(\psi)$ gets empty (bottom right of Figure 8). Thus, $\partial G_2 / \partial \psi_3(\psi)$ is not continuous. Newton's method requires a certain regularity, and we will see below that it converges under the above genericity assumptions.
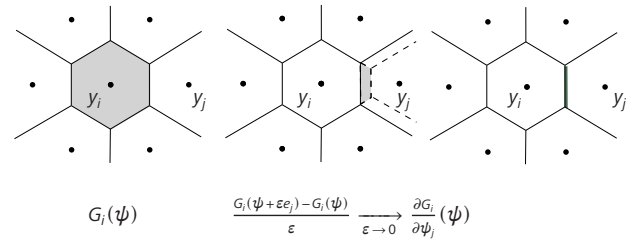


$$G_i(\psi) \qquad \frac{G_i(\psi + \varepsilon e_j) - G_i(\psi)}{\varepsilon} \xrightarrow[\varepsilon \to 0]{} \frac{\partial G_i}{\partial \psi_j}(\psi)$$

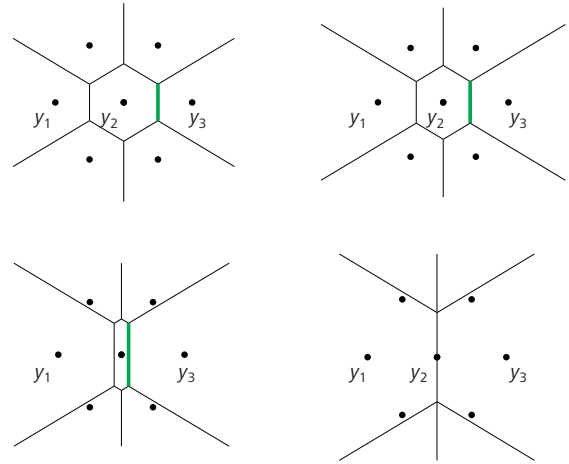*Figure 7.* The partial derivatives are boundary integrals



*Figure 8.* Non-continuous partial derivative: $\partial G_2 / \partial \psi_3$ is an integral on the green segment $\mathrm{Lag}_{23}$ which is discontinuous.

To establish the convergence of Newton's method, we also need to study the concavity of the Kantorovitch functional $\mathcal{K}$, or equivalently the monotonicity of its gradient $\nabla \mathcal{K} = G - \nu$. The functions $\mathcal{K}$ and $G$ are invariant by addition of a constant vector (i.e., $\mathcal{K}(\psi + C(1, \ldots, 1)) = \mathcal{K}(\psi)$), which can be seen in the definition of Laguerre cells. Thus, we can only hope to establish strong concavity of $\mathcal{K}$ in the directions orthogonal to constant vectors, i.e., belonging to the set

$$\mathcal{M}_0 := \Big\{ v \in \mathbb{R}^N \mid \sum_{1 \leq i \leq N} v_i = 0 \Big\}.$$

Another reason for the lack of strong concavity of $\mathcal{K}$ is that if $\psi_i$ is very large, then $\mathrm{Lag}_i(\psi)$ is empty and remains empty in a neighborhood of $\psi$. In this case, $G_i(\psi)$ is constant equal to zero, and the Hessian matrix $D^2 G(\psi) = DG$ has a row of zeros. We can therefore hope to establish strong concavity only if $\psi$ belongs to the set

$$\mathcal{C}_+ := \{ \psi \in \mathbb{R}^N \mid \forall i, \ G_i(\psi) > 0 \}.$$

The next theorem shows, in a nutshell, that these are the only two obstructions to strong concavity.

**Theorem 3.5** (Strict concavity). *We assume the hypotheses of the previous theorem hold. If the set $\{\rho > 0\}$ is connected, the function $\mathcal{K}$ is locally strongly concave on $\mathcal{C}_+$ in the direction $\mathcal{M}_0$:*

$$\forall \psi \in \mathcal{C}_+, \ \forall v \in \mathcal{M}_0 \setminus \{0\}, \quad \langle DG(\psi)v \,|\, v \rangle < 0.$$

**Remark 3.3** (Uniqueness). We saw above that the function $\mathcal{K}$ has a maximum, and thus equation (MA) has a solution. The previous theorem implies that this maximum is unique if we impose that $\psi \in \mathcal{M}_0$, i.e., $\psi$ has zero average, since a strictly concave function admits at most one local maximum.

We will see in the next paragraph how these results of regularity and monotonicity allow us to iteratively construct a sequence $(\psi^{(k)})_{k \geq 0}$ converging to the unique zero-average $\psi^*$ satisfying $G(\psi^*) = \nu$.

### 3.5 Newton's method

*Newton's method in 1D*

We begin by recalling Newton's method for solving the equation $g(x) = 0$, where $g : \mathbb{R} \to \mathbb{R}$ is a real function. Newton's method starts from $x_0 \in \mathbb{R}$ and constructs the sequence $x^{k+1} = x^k - g(x^k)/g'(x^k)$ by induction. If we assume that $g$ is of class $\mathcal{C}^1$ and that there exists $a \in \mathbb{R}$ such that $g(a) = 0$ and $g'(a) \neq 0$, then one can show, using Taylor–Lagrange formulas, that for $x^0$ sufficiently close to $a$, the sequence $(x^k)_{k \geq 0}$ converges to $a$. The convergence is then said to be local. Thus, under a regularity hypothesis ($g \in \mathcal{C}^1$) and monotonicity ($g'$ has constant sign in a neighborhood of $a$), Newton's method converges locally.

*Newton's method (local)*

Assume that we are given a zero-average vector $\psi^0 \in \mathcal{M}_0$ such that the mass of all Laguerre cells is strictly positive:

$$\varepsilon_0 := \frac{1}{2} \min \left[ \min_{y \in Y} G_i(\psi^0), \ \min_{1 \leq i \leq N} \nu_{y_i} \right] > 0.$$

We define $\psi^{k+1}$ in the following way: we start by calculating the Newton direction $d^k$, i.e., the vector $d^k$ satisfying

$$DG(\psi^k)d^k = -(G(\psi^k) - \nu) \quad \text{and} \quad d_i^k \in \mathcal{M}_0,$$

which exists and is unique by according to Theorem 3.5. The second equation enables us to overcome the invariance of $G$ and thus the non-invertibility of $DG(\psi^k)$. We then define $\psi^{k+1} = \psi^k + d^k$. As in the 1D case, it can be shown that the method converges locally: if $\psi^0$ is chosen close enough to the $\psi^*$ solution, then the sequence $(\psi^k)$ converges to $\psi^*$.

*Globally convergent Newton's method*

However, the condition $\psi^0$ is close to the solution $\psi^*$ is impossible to fulfill in practice. Fortunately, a very simple modification of the method allows to ensure a global convergence, allowing us to drop this closeness assumption. To do this, one must construct $\psi^{k+1}$ in such a way that the kernel of the Jacobian $DG(\psi^{k+1})$ remains equal to constant vectors, so that the system defining the direction $d^{k+1}$ admits a unique solution. For this purpose, we define the *step $\tau^k$* as the largest real of the form $2^{-\ell}$ (with $\ell \in \mathbb{N}$) such that $\psi^{k,\ell} := \psi^k + 2^{-\ell}d^k$ satisfies

$$\begin{cases} \forall i \in \{1, \dots, N\}, \quad G_i(\psi^{k,\ell}) \geq \varepsilon_0, \\ \|G(\psi^{k,\ell}) - \nu\| \leq (1 - 2^{-(\ell+1)})\|G(\psi^k) - \nu\|. \end{cases}$$

Finally, we define $\psi^{k+1} = \psi^k + \tau^k d^k$.

By using the regularity and concavity results on $\mathcal{K}$, the step $\tau^k$ can be bounded from below, thus ensuring the convergence of the sequence constructed above to a solution of the optimal transport problem [4]:

**Theorem 3.6.** *Under the assumptions of Theorem 3.5, there exists $\tau^* > 0$ such that*

$$\|G(\psi^{k+1}) - \nu\| \leq \left(1 - \frac{\tau^\star}{2}\right)\|G(\psi^k) - \nu\|.$$

*In particular, the sequence $(\psi^k)_{k \geq 0}$ converges to the unique solution $\psi^*$ of (MA) satisfying $\sum_i \psi_i^* = 0$.*

**Remark 3.4** (Quadratic convergence). The above theorem shows that the convergence of Newton's method is globally exponential. This convergence is actually called *linear convergence* in optimization. When the cost $c$ satisfies the *Ma–Trudinger–Wang* (MTW) condition that appears in the theory of optimal transport regularity, and the density $\rho$ is Lipschitz, then the convergence is even locally quadratic [3]: for sufficiently large $k$, we have

$$\|G(\psi^{k+1}) - \nu\| \leq \frac{1}{2}\|G(\psi^k) - \nu\|^2.$$

In practice, the convergence is very fast and the basin where quadratic convergence occurs seems to be quite large. This last observation is empirical, and not mathematically explained yet. In Figure 9, $X = [0,1]^2$ is the large white square and $Y$ is a set of points in the lower left corner and $c(x,y) = \|x - y\|^2$. With $N = 100$ points, after three iterations the error $\|G(\psi^3) - \nu\|_1$ is already of order $10^{-9}$. Even difficult examples of size $N = 10^7$ in dimension $d = 3$ can be solved to high numerical precision with less than 20 iterations!

## 4 Applications to anidolic optics

In this section we present the adaptation of semi-discrete methods to the practical resolution of inverse problems in optics. These results were obtained in the PhD thesis of Jocelyn Meyron and the images are taken from the article [5].
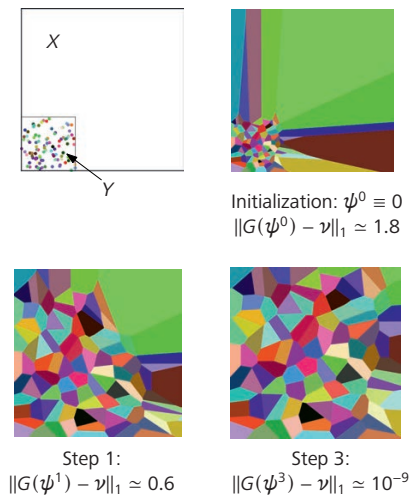
Initialization: $\psi^0 \equiv 0$
$\|G(\psi^0) - \nu\|_1 \simeq 1.8$

Step 1:
$\|G(\psi^1) - \nu\|_1 \simeq 0.6$

Step 3:
$\|G(\psi^3) - \nu\|_1 \simeq 10^{-9}$

*Figure 9.* Convergence of the sequence $(\psi^k)$. On images 2, 3 and 4 we see the Laguerre cells $\text{Lag}_i(\psi^k)$ for $k=0,1,3$.

### 4.1 Far-field problems

We saw in Section 2 that in several far-field problems, i.e., when the target illumination is at infinity, solving the Monge–Ampère equation (MA) allows us to construct an optical component. This involves modelling mirrors or lenses, with a point or collimated light source, and in each case there are two components that may be produced (one of which is convex), so that in all we have formulated eight different near-field optical problems.

The main difficulty in implementing Newton's algorithm to solve (MA) lies in the evaluation of the function $G$ and its differential $DG$ at point $\psi^k$, and more precisely in the calculation of the set of Laguerre cells $\text{Lag}_i(\psi^k)$. For cells from non-imaging optics problems, also called visibility cells, it is possible to perform this calculation in almost linear time in the number $N$ of Dirac masses. Take for example the mirror problem for a point source. The visibility cells are obtained by projecting radially onto the sphere an intersection of "solid" confocal paraboloids, and we have already seen that the intersection of two confocal paraboloids is included in a plane. Another simple calculation shows that the radial projection of such an intersection is also included in a (different) plane. This shows that the visibility cells are separated by hyperplanes. In fact, it can be shown that there exists a partition of $\mathbb{R}^3$ into convex polyhedra $P_1, \ldots, P_N$ – called a *power diagram* in computational geometry – such that each visibility cell is of the form $V_i(\psi) = \mathbb{S}^2 \cap P_i$ (Figure 10). A similar property holds for each of the eight problems. The point of this reformulation is that there are powerful libraries – for example CGAL or GEOGRAM – that allow us to compute power diagrams in dimensions 2 and 3, and thus also the Laguerre cells associated with the optics problems. It is therefore possible to implement the damped Newton algorithm, and to use it to construct – numerically and even physically – mirrors and lenses for far-field targets in anidolic optics.
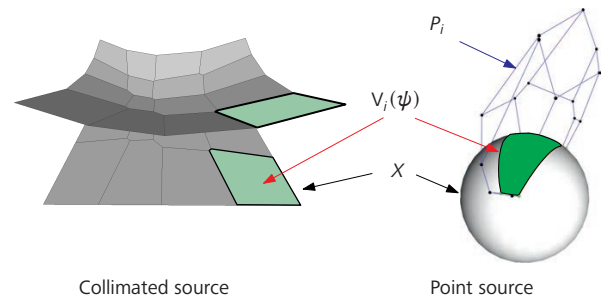


Collimated source

Point source

*Figure 10.* Visibility cell structure

### 4.2 Near-field problems

It is also possible to deal with more realistic target illuminations in the *near-field* – i.e., when illuminating points at a finite distance rather than directions – with an iterative method that solves a far-field solution at each step [5]. The convergence is very fast, requiring only a few iterations, as illustrated in Figure 11.

In all the experiments presented below, the light source is assumed to be uniform, so that the light source $\mu$ has a constant density on its support. The reflection or refraction of this light on a wall is simulated in the computer by the physically realistic rendering software LuxRender.

*Generic method*

The different problems of anidolic optics having the same structure (point or collimated light sources, mirrors or lenses, convex or concave components, near-field or far-field), it is possible to solve them in a unified, precise and automatic manner with the same
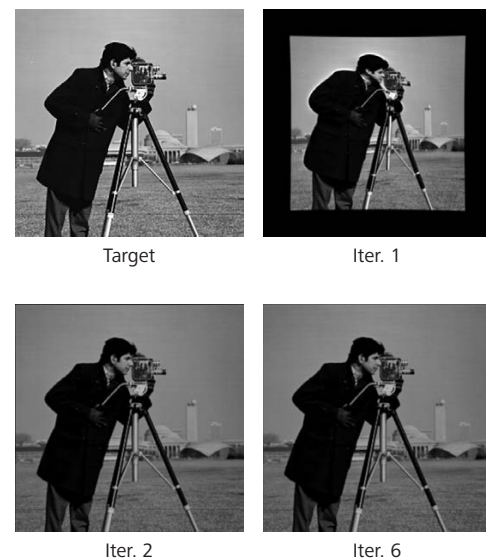


Target

Iter. 1

Iter. 2

Iter. 6

*Figure 11.* Convergence of far-field mirrors to near-field mirrors
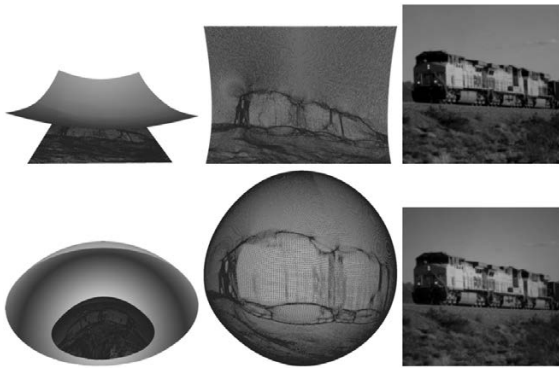
Figure 12. Mirrors for collimated (top) and point (bottom) light; visibility cells (left), component mesh (middle) and rendering with LUXRENDER (right)
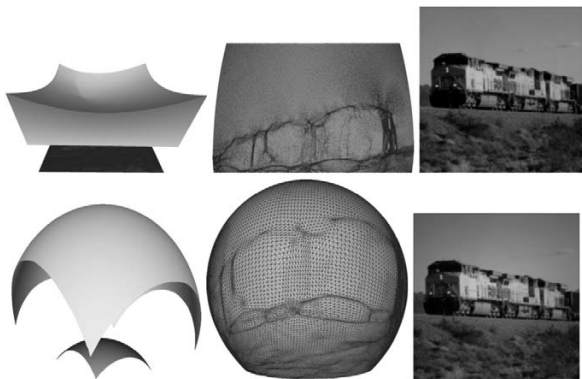


Figure 13. Lenses for collimated (top) and point (bottom) light; visibility cells (left), component mesh (middle) and rendering with LUXRENDER (right)
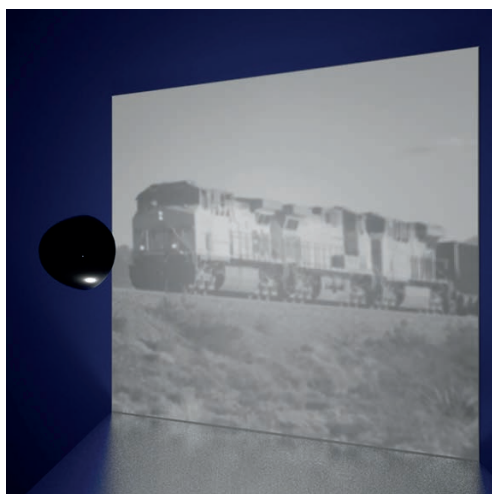


Figure 14. A point light (not visible) is placed in front of the mirror and the path of the light is simulated by the computer using the physically realistic renderer LUXRENDER
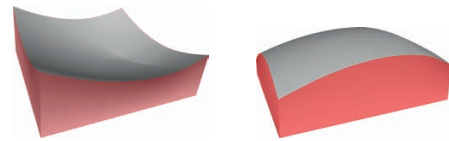


Figure 15. Concave and convex lenses

algorithm (Figures 12, 13 and 14). In Figures 12 and 13, the visibility cells on the sphere or plane are shown on the left, above which is the surface of the optical component. Each surface is represented in the computer by a mesh (a set of triangles) which is shown in the middle. The simulation of the reflected or reflacted light with LUXRENDER is on the left.

### Convexity/concavity of the components

Some applications require the construction of optical components with convexity properties. This is the case in the automotive industry for the construction of mirrors and/or lenses. The reason for this is both practical, as it is easier to build a convex component, and aesthetic. In the case of collimated light sources, mirrors or lenses can always be convex or concave, as can be seen in Figure 15.

### Singularity of solutions

The optical components are by construction objects with only a $\mathcal{C}^0$ regularity. Indeed, they are surfaces composed of pieces of planes, paraboloids or ellipsoids (in the case of a mirror for a point light source) which are joined together in a manner that is continuous but not $\mathcal{C}^1$. However, as the discretization of the target illumination becomes finer and finer, the surface tends towards an object that has greater regularity. In Figure 16, we observe a $\mathcal{C}^1$ regularity, except at points on the surface that correspond to black areas in
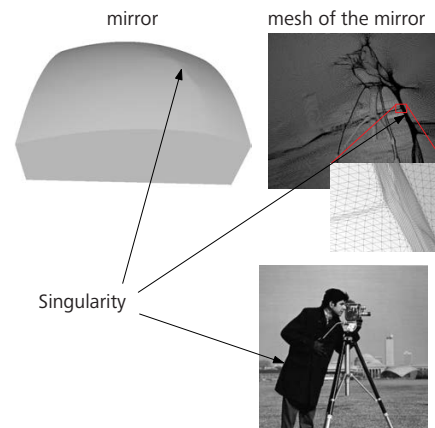


Image rendered with LUXRENDER

Figure 16. Singularity and meshing (surface singularities correspond to black areas)

the target image. Intuitively, the lack of regularity comes from the fact that the light must avoid the black areas, which results in a jump in the vector field normal to the surface.

*Pillows*

The inner part of a car headlamp is typically made up of "pillows", i.e., several small components. Each patch is intended to illuminate a fairly wide range of directions, and the lights sent out by each pillow overlap. This ensures a certain robustness in the lighting. If for instance a bird flies past the headlights, not too close, it does not obstruct all the light and the road remains fully illuminated. In Figure 17, the target illumination for each pillows is the cameraman's image. When the calculations are done in the far-field, i.e., when illuminating directions, the images are superimposed, but with an offset due to the size of the pillows. To obtain a clear image, it is necessary to make the calculations in the near-field, so as to illuminate exactly the desired points. Note that the target is always illuminated even if an obstacle, for example a red monkey head, is placed in front of some of the pillows.

*Colored target illumination*

Similarly, solving the near-field problem makes it possible to illuminate a target in color. Indeed, one can build an optical component for each channel (red, green and blue). Then each of the three lights is sent to its associated component and the colors are added to the target to form a color image. This is done in Figure 18 with three lenses.

*Construction of mirrors and lenses*

We also built optical components. The lenses and mirrors in Figures 19, 2 and 21 were milled by the GINOVA technology platform in Grenoble on a 3-axis CNC (*computer numerical control*) machine with 10 mm radius milling cutters. The path of the milling cutter creates irregularities on the optical components (Figure 22). Note that the convexity of the optical components allows the use of arbitrarily large milling radii, which reduces machining irregularities. In any case, it is necessary to grind under water and then polish the optical components (Figure 23). Of course, this affects the optical quality and tends to whiten the black areas in the target image.

Figure 17. Lens composed of 9 pillows: In the far-field (top); in the near-field (middle); with obstacle (bottom)
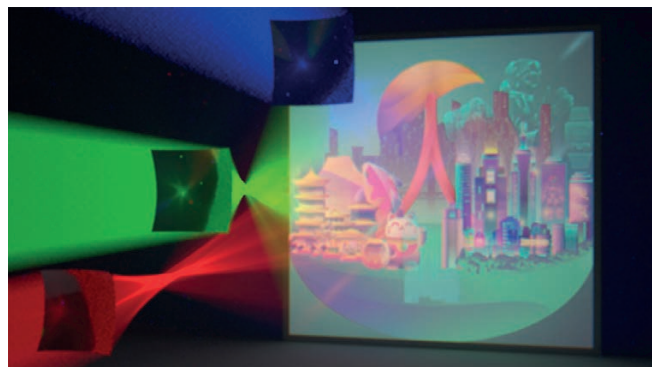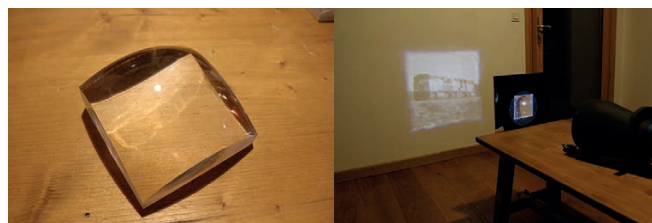


Figure 18. Color image



Figure 19. Lens transforming collimated light into the picture of a train
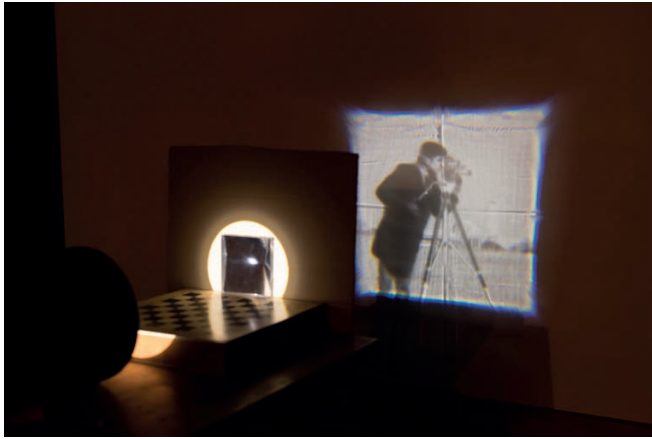
*Figure 20.* Lens transforming collimated light into the picture of a cameraman



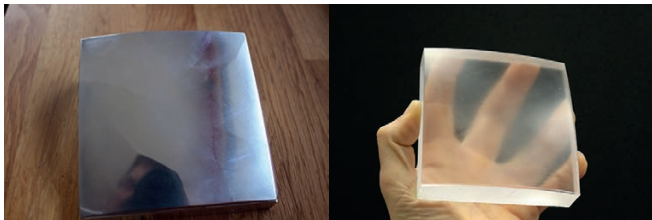*Figure 21.* Mirror transforming collimated light into the picture of a cameraman



*Figure 22.* Mirrors and lenses after machining



*Figure 23.* Sanding and polishing by hand

## References

[1] L. Caffarelli and V. Oliker, Weak solutions of one inverse problem in geometric optics. *Journal of Mathematical Sciences* **154**, 39–49 (2008)

[2] P. Guan and X.-J. Wang, On a monge-ampere equation arising in geometric optics. *J. Differential Geom* **48**, 205–223 (1998)

[3] J. Kitagawa, Q. Mérigot and B. Thibert, Convergence of a Newton algorithm for semi-discrete optimal transport. *Journal of the European Mathematical Society* (2019)

[4] Q. Mérigot and B. Thibert, Optimal transport: Discretization and algorithms. In *Handbook of Numerical Analysis, Geometric PDEs* 22, Elsevier, 621–679 (2020)

[5] J. Meyron, Q. Mérigot and B. Thibert, Light in power: A general and parameter-free algorithm for caustic design. In *SIGGRAPH Asia 2018 Technical Papers*, ACM Transaction on Graphics, p. 224 (2018)

[6] X.-J. Wang, On the design of a reflector antenna. *Inverse Problems* **12**, 351–375 (1996)

Quentin Mérigot is a professor in applied mathematics at Université Paris-Saclay. His work combines optimal transport and computational geometry to solve numerically partial differential equations and inverse problems.

quentin.merigot@universite-paris-saclay.fr

Boris Thibert is an associate professor in applied mathematics at Université Grenoble Alpes. He is working on the numerical aspects of optimal transport, Monge-Ampère equations and convex integration theory.

boris.thibert@univ-grenoble-alpes.fr